Fluid Dynamics Research 11 (1993) 37–59
North-Holland

FLUID DYNAMICS
RESEARCH

Determining the effective viscosity of a carbon paste used for continuous electrode smelting

A.D. Fitt [a] and J.M. Aitchison [b]

[a] *Faculty of Mathematics, University of Southampton, SO9 5NH, UK*
[b] *Applied and Computational Mathematics Group, Royal Military College of Science Shrivenham, Swindon SN6 8LA, UK*

Received 22 January 1992
Revised manuscript received 4 May 1992

Abstract. The Soderberg electrode is a continuously consumed smelting electrode used in the production process of materials such as ferroalloys. The material which makes up the electrode is composed of a carbon "paste" which is solid at room temperature but softens, flows and is finally baked with increasing temperature. Although the carbon paste is in reality a two-phase mixture, there is much industrial interest in determining its "effective" viscosity. Traditionally this has been accomplished using a variety of laboratory tests which involve subjecting a paste sample to prescribed loads or displacements and measuring changes in the geometric properties of the sample. The aim of the current study is to predict the effect viscosity of a paste sample by predicting the "bulging" of a sample. Mathematical models are proposed for these procedures and it is shown that a slow-flow treatment is applicable. Certain sample geometries permit an analytic treatment of the problem, where exact solutions for the small-time behaviour of the regions of the sample away from its boundary may be determined. It is further shown that the behaviour of the solution near to the boundaries may be determined using a boundary layer analysis, and leads to a non-canonical end problem which may be solved by employing Papkovitch–Fadle eigenfunction expansions. The finite element method is used to derive numerical solutions which confirm the predictions of the model for the effective viscosity of the sample. Finally, some numerical solutions are given for more general geometries where analytic solutions are not available.

1. Introduction

Electric smelting is currently used in a number of countries to produce a variety of materials such as ferroalloys, silicon metal and calcium carbide. For the industrial process to operate successfully, large amounts of energy must be transported to the heart of the smelting furnace where the end product is created in molten form. In the process discussed below, the energy is provided in the form of substantial electric currents that are passed along a carbon electrode. The electrode is continuously consumed in the smelting process, moving a distance of order 1 m per day, and must therefore be replenished. One possibility for replenishment would be to add pre-formed electrode segments to the top of the electrode, but a more practical solution is to produce a continuous carbon electrode immediately above the furnace. To accomplish this, cylinders of carbon paste are fed into the centre of the cylindrical steel casing (of diameter 1–2 m) which is heated gradually. Under heating, the paste flows to fill the whole cylinder and is finally baked at about 500°C in the region where the current enters the electrode. Such an electrode is called a Soderberg electrode.

Correspondence to: A.D Fitt, Faculty of Mathematics, University of Southampton, SO9 5NH, UK.

This paper concerns the problem of determining the effective viscosity of the carbon paste, which is composed of a mixture of particles and binder. In most applications, the binder is pitch or tar, and the particles are composed of calcinated anthracite (coke). The coke particles may have diameters ranging from less than 125 μm to 15 mm, so that although the binder may be considered to behave like a Newtonian fluid, the paste mixture exhibits complicated rheological characteristics. The behaviour of the paste is also highly temperature dependent. At room temperature the paste is solid, but at 50–80°C it begins to soften. Thereafter the flowability increases with increasing temperature. This property of the paste has been measured using a viscometer at temperatures up to 225°C. A further complication is introduced by the fact that the solid particles are present in the paste in very high concentrations, experience showing that to achieve a paste with suitable flow characteristics as well as low resistivity and high strength, the required particle concentration is typically 70–75%. A consequence of this is that particle/particle contact becomes important, and granular and frictional effects are observed. It is also possible for the paste to segregate, so that the binder and particles constituents separate and the material is no longer uniform. Segregation is usually observed along the steel casing close to the point where the current enters, and can give rise to poor quality electrodes which may subsequently break.

Clearly the description of the flow of the carbon paste within the electrode requires a major modelling effort if it is to be well understood and accurately predicted. Rather than attempt to do this, attention in the past has fixed on producing a paste with an appropriate effective viscosity (flowability), treating the binder/particles mixture as though it was a single component viscous fluid, the chosen level of apparent viscosity being based on experience. The main reason for this approach is that the paste flow in the upper part of the electrode is so complicated that most existing mathematical models for predicting the motion and consumption of the Soderberg electrode are based on standard fluid mechanics equations containing only a single viscosity (see, for example Bergstrom et al. (1989)). Although this viscosity is highly temperature-dependent, no explicit mention is made of the separate components of the pitch–particles mixture. Our aim is therefore to examine, both analytically and numerically, the processes by which the effective viscosity of the paste (at a given, constant prescribed temperature) may be determined.

We shall consider three sorts of viscosity test that might be applied to a block of carbon paste. Firstly, a block of paste is heated (normally to about 300°C), placed on a rigid impermeable solid surface and left to slump under its own weight. Thereafter the viscosity is inferred from the resulting shape of the block. This experiment has come to be known as the "plasticity" test (a slightly misleading name since no plasticity in the normal sense of the word is involved, but one which we shall use henceforth in deference to the standard terminology of the industry) and may take many minutes to complete. Two other somewhat faster forms of test which are in common use are similar in spirit to the plasticity test, but involve a metal plate which is applied to the (plane) top surface of the sample. The plate is then forced to move either with a prescribed (often constant) velocity (the "velocity test") or with a prescribed force (the "viscometer"). Again, we shall use the terminology as described, but of course both the latter two tests are viscometers. Mathematically, the only difference between the plasticity test, the viscometer and the velocity test is the boundary condition that is applied on the top surface of the test sample. The aim in all three cases is to predict the "bulging" of an experimental sample and thereby infer the effective viscosity of the material.

2. Mathematical model

To fix our ideas, we consider a two-dimensional block of paste occupying a region D which is initially rectangular with height h and semi-width L. Rectangular cartesian coordinates

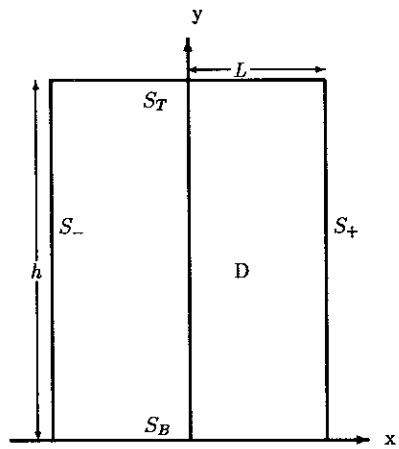

Fig. 1 Geometry of paste sample.

with unit vectors $\boldsymbol{i}$, $\boldsymbol{j}$ and $\boldsymbol{k}$ ($\boldsymbol{k}$ pointing out of the paper) are employed, and the top surface of the sample is denoted by S_T, the surface in contact with the rigid plane $y = 0$ by S_B, and the (initially vertical) sides of the sample by S_+ and S_-. (See fig. 1.)

Assuming that the temperature is constant and non-dimensionalizing lengths with h, the fluid velocity $\boldsymbol{q}$ with U_∞ where U_∞ is some representative speed (for example, the speed of the centre of the top of the sample), the time t with T, a typical time scale, and the pressure p and the stress tensor $\mathbf{T}$ with $\mu U_\infty/h$ where μ is the viscosity to be determined, the Navier–Stokes equations with body force become, in non-dimensional variables,

$$\mathrm{Re}\left[\mathrm{St}^{-1}\boldsymbol{q}_t + (\boldsymbol{q}\cdot\nabla)\boldsymbol{q}\right] = -\nabla p + \nabla^2\boldsymbol{q} - (\mathrm{Re}/\mathrm{Fr})\boldsymbol{j}, \quad \nabla\cdot\boldsymbol{q} = 0,$$

where subscripts denote differentiation and as usual the Reynolds, Froude and Strouhal numbers are defined by

$$\mathrm{Re} = \frac{hU_\infty\rho}{\mu}, \quad \mathrm{Fr} = \frac{U_\infty^2}{gh}, \quad \mathrm{St} = \frac{TU_\infty}{h}.$$

Since none of the viscosity tests involve impulsive loadings, we assume that the Strouhal number is order unity so that $U_\infty \sim h/T$. Taking typical values for the variables of $h \sim 1$ m, $U_\infty \sim 1$ m/h (almost certainly an overestimate, even for the velocity test), $\rho \sim 3$ g/cm^3, and a value for the viscosity of 10^8 Pa s gives

$$\mathrm{Re} = \mathrm{O}(10^{-8}), \quad \mathrm{Fr} = \mathrm{O}(10^{-8})$$

so that to lowest order the non-dimensional equations of motion become

$$\nabla p = \nabla^2\boldsymbol{q} - \alpha\boldsymbol{j}, \quad \nabla\cdot\boldsymbol{q} = 0, \tag{1}$$

where $\alpha = \mathrm{Re}/\mathrm{Fr}$, and we simply retrieve the slow flow equations with a body force. Admittedly the order of magnitude variations in the viscosity will mean that under some circumstances the Reynolds and Froude numbers will not be comparable, but the convective terms in the Navier–Stokes equations will always vanish to lowest order because of the low velocities. As far as the boundary conditions are concerned, the sides S_+ and S_- are stress-free, there is a standard no-slip condition on S_B, and the top of the sample S_T is either stress-free (plasticity test), has given velocity (velocity test) or a given total normal stress with a horizontal boundary (viscometer).

As usual, we may take the curl of the momentum equation and identically satisfy the continuity equation by defining a stream function ψ such that $u = \psi_y$, $v = -\psi_x$, so that ψ satisfies the biharmonic equation in D. When the boundary conditions are expressed in terms of the stream function the full non-dimensional problem may conveniently be written

$$\nabla^4\psi = 0 \quad ((x, y) \in \mathrm{D}), \quad \psi = \psi_y = 0 \quad ((x, y) \in \mathrm{S_B}),$$

$$\mathbf{T}\cdot\boldsymbol{n} = 0 \quad ((x, y) \in \mathrm{S_+ \cup S_-})$$

$$(\mathrm{D}/\mathrm{D}t)[x - \xi(y, t)] = 0 \quad ((x, y) \in \mathrm{S_+ \cup S_-}),$$

$$\left.\begin{array}{ll} \mathbf{T}\cdot\boldsymbol{n} = 0 & \text{(plasticity test)} \\ \psi_y = 0, \quad \psi_x = -\dot{s}(t) & \text{(velocity test)} \\ \psi_y = 0, \quad -p - 2\psi_{xy} = \gamma(t) & \text{(viscometer)} \end{array}\right\} (x, y) \in \mathrm{S_T}. \tag{2}$$

Here $\mathrm{D}/\mathrm{D}t$ denotes the standard convective derivative, $\boldsymbol{n}$ is the unit normal to the boundary and $\dot{s}(t)$ and $\gamma(t)$ represent a non-dimensionalized velocity and normal stress respectively. Also, we have denoted the (non-dimensional) equation of the boundary $\mathrm{S_+}$ by $x = \xi(y, t)$. Time enters into the problem via the standard kinematic boundary condition on the free surfaces of the sample and the body force term will enter via the pressures which appear in the boundary conditions. Clearly the problem as posed at present will be too hard to solve analytically and numerical methods will have to be used. Before describing the numerical procedure however, we consider some circumstances in which some analytic progress may be made.

2.1 Corner solutions

Some headway may be made by examining the behaviour in the corners of the block. These corners fall into four categories depending on the boundary conditions on the two adjoining sides. For the velocity test and the viscometer these boundary conditions are similar at the top and bottom. We therefore confine our attention to the plasticity test. If we denote by x and y the horizontal and vertical coordinates centered at each corner in turn then, ignoring any possible eigenfunctions, we find the following local behaviour.

(i) At a top corner (where two stress free surfaces meet)

$$u \sim -\tfrac{1}{4}\alpha xy, \quad v \sim \tfrac{1}{8}\alpha(x^2 + y^2), \quad p \sim -\tfrac{1}{2}\alpha y.$$

(ii) Near the line of symmetry at the top,

$$u \sim \alpha\beta xy, \quad v \sim -\tfrac{1}{2}\alpha\beta(x^2 + y^2), \quad p \sim \alpha(-1 - 2\beta)y$$

(where β is arbitrary and would have to be determined by matching with the outer solution).

(iii) At a bottom corner (where a stress free surface meets a fixed surface)

$$u \sim -\tfrac{1}{3}\alpha xy, \quad v \sim \tfrac{1}{6}\alpha y^2, \quad p \sim -\tfrac{2}{3}\alpha y.$$

(iv) Near the bottom line of symmetry

$$u \sim \alpha\delta xy, \quad v \sim -\tfrac{1}{2}\alpha\delta y^2, \quad p \sim \alpha(-1 - \delta)y,$$

where δ is arbitrary.

Interestingly, in each case these local solutions produce no outward motion of the free surfaces and hence no bulging. To produce the observed bulging it is necessary to recognize that the flow is dominated by an eigensolution. A local analysis indicates that, by including eigensolutions, bulging may occur near the bottom corners but not at the top corners. With or

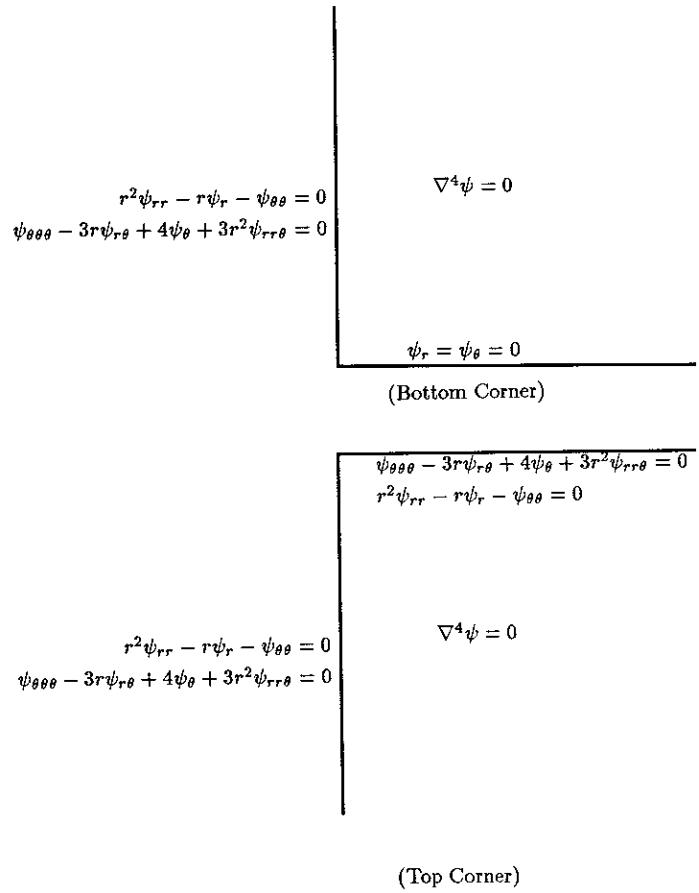

Fig. 2. Quarter plane eigenproblems

without eigensolutions the bottom cornerpoint does not move. In the absence of surface roughness this is due to the no slip boundary conditions applied at y = 0, and does not occur if they are removed (see for example the analogous problem for inviscid flow which was studied by Penney and Thornhill (1952)).

To examine the local behaviour of the eigensolutions near the corners we consider the two quarter space problems shown in fig. (2) and seek solutions of the form

$$\psi = r^\lambda[A \cos \lambda\theta + B \sin \lambda\theta + C \cos(\lambda - 2)\theta + D \sin(\lambda - 2)\theta]$$

For the bottom corner it is found that $\lambda = 1$ (so that $\psi \propto r \sin \theta$ and thus u is zero along $\theta = \pi/2$), or

$$\tan^2(\pi\lambda/2) = (\lambda - 1)^2/\lambda(2 - \lambda),$$

which has precisely two real solutions $\lambda \approx 0.405$, which we reject since it leads to a singularity in u at $r = 0$, and $\lambda \approx 1.595$. Therefore an eigensolution with a velocity along $\theta = \pi/2$ of

$$\partial\psi/\partial r \sim r^{0.6}$$

is possible. This allows bulging and suggests a free boundary which grows like $tr^{0.6}$. The equivalent condition near the top corner is

$$\tan^2(\pi\lambda/2) = \lambda(\lambda - 2)/(\lambda - 1)^2,$$

which only possesses real solutions $\lambda = 0, 1, 2$. All of these values again give $u = 0$ on $\theta = \pi/2$ and therefore do not permit bulging.

3. Geometries which admit an analytical solution

The corner solutions discussed above provide qualitative information concerning the "bulging" of the sample, but inevitably contain constants that must be determined from matching with an unknown solution, and so do not allow predictions of the viscosity to be made. In this section we consider a sample shape which simplifies the problem to such an extent that estimates for the viscosity may be directly determined.

3.1 A tall, thin sample

We analyze first the case of a tall, thin paste block where $L/h = \epsilon \ll 1$. We shall consider the region $x > 0$ and impose symmetry conditions on $x = 0$. Having made the further obvious scalings $x = \epsilon X$, $u = \epsilon U$ and $\xi = \epsilon\eta$, the scaled non-dimensional problem (1) becomes

$$p_X = U_{XX} + \epsilon^2 U_{yy}, \quad \epsilon^2 p_y = v_{XX} + \epsilon^2 v_{yy} - \epsilon^2\alpha, \quad U_X + v_y = 0.$$

If we now write $U = U_0 + \epsilon U_1 + \epsilon^2 U_2 + \cdots$ and use similar expansions for v, p and η, then it is easy to show that solutions which satisfy the differential equations and the symmetry conditions $U = v_X = 0$ on $X = 0$ are given up to $O(\epsilon^2)$ by

$$U = -Xv_{0y} - \epsilon X v_{1y} + \epsilon^2\left[-\tfrac{1}{6}X^3(-2v_{0yyy} + g_{0yy}) - Xq_y\right],$$

$$v = v_0(y, t) + \epsilon v_1(y, t) + \epsilon^2\left[\tfrac{1}{2}X^2(g_{0y} + \alpha - 2v_{0yy}) + q(y, t)\right],$$

$$p = (-v_{0y} + g_0) + \epsilon(-v_{1y} + g_1) + \epsilon^2\left[\tfrac{1}{2}X^2(v_{0yyy} - g_{0yy}) + g_2(y, t)\right],$$

where the functions $q(y, t)$, $g_1(y, t)$, $g_2(y, t)$ and $g_3(y, t)$ remain to be determined. Imposing the free surface kinematic boundary condition to leading order gives an equation for η_0 and v_0 which is

$$\dot{\eta}_0 + (\eta_0 v_0)_y = 0,$$

the dot representing a time derivative. Clearly another equation for η_0 and v_0 is required and this can be derived by imposing the stress-free conditions on the scaled boundary $X = \eta(y, t)$. Setting the x-component of $\mathbf{T} \cdot \boldsymbol{n}$ equal to zero gives

$$-g_0 - v_{0y} = -g_1 - v_{1y} = 0,$$

whilst the order ϵ^2 contribution relates the functions q, g_2 and g_3. The y-component yields nothing until we reach the order ϵ^2 terms, whereupon we find that

$$4(\eta_0 v_{0y})_y = \alpha\eta_0.$$

The solution of the leading order problem may therefore be written

$$v = v_0(y, t) + \epsilon v_1(y, t) + \epsilon^2\left[\tfrac{1}{2}X^2(\alpha - 3v_{0yy}) + q(y, t)\right],$$

$$U = -Xv_{0y} - \epsilon X v_{1y} + \epsilon^2\left[\tfrac{1}{2}X^3 v_{0yyy} - Xq_y\right],$$

$$p = -2v_{0y} - 2\epsilon v_{1y} + \epsilon^2\left[X^2 v_{0yyy} + g_2\right],$$

$$\text{where} \quad \dot{\eta}_0 + (\eta_0 v_0)_y = 0, \quad 4(\eta_0 v_{0y})_y = \alpha\eta_0. \tag{3}$$

Some thought needs to be given to the boundary conditions of the equations for η_0 and v_0. In general we would expect to be able to specify two boundary conditions for v_0 and an initial condition for η_0 when solving the leading order problem. Therefore it will not be possible to force the leading order solution to satisfy two no-slip conditions on $y = 0$ and two stress or velocity conditions on $y = s(t)$. There will be locations near to the top and/or the bottom of the sample where inner expansions will be required to determine the correct behaviour. We therefore regard the leading order problem formulated above as an "outer" problem.

Again, there are the usual three viscosity tests which we could consider to give different boundary conditions on the top surface. We must choose two out of four possible conditions for v_0 to satisfy. Since we would like the outer problem to reflect properties of both the top and bottom of the sample, we choose to satisfy the condition $v_0 = 0$ on $y = 0$ and one condition on $y = s(t)$. It is worth mentioning that for the velocity test it is possible to specify two conditions on $y = s(t)$ and none on the base of the sample, but evidently this is physically the wrong approach.

A general comment concerning the equations for η_0 and v_0 is in order here: a standard characteristic analysis shows that the characteristics of the system are given by

$$dt/dy = 0, \quad 0, \quad \text{and} \quad 1/v_0.$$

The fact that there is only one non-trivial characteristic arises from the absence of any time derivatives of v_0. Consequentially, it must be noted that if we wish to prescribe the vertical velocity v_0 along any curve $y = s(t)$, then the consistency condition along the non-trivial characteristic demands that $v = \dot{s}$. So a prescription of the vertical velocity at the top of the sample amounts to characteristic data, but of a consistent form.

Equations (3) may be solved numerically in a variety of efficient ways; one attractive possibility involves a change of the independent variable y of the form $\bar{y} = y/s(t)$ which has the effect of conveniently fixing the moving boundary. Since the full equations will be solved numerically in section 4 however, we do not pursue this further.

Before further analysing the individual experiments, it is worth mentioning that, though we have proceeded using asymptotic analysis, the second eqs. (3) may also be arrived at using a simple physical argument which is normally referred to as the "Young experiment". The components t_{xx} and t_{yy} of the stress tensor are given by $t_{xx} = -p + 2u_x$ and $t_{yy} = -p + 2v_y$. Near the stress-free side of the sample where $t_{xx} = 0$ and $u_x + v_y = 0$ this yields $t_{yy} = 4v_y$. The second of eqs. (3) therefore amounts to an assertion that the rate of change of the total force ηt_{yy} exerted by this stress over the surface η must exactly balance the weight of a layer.

3.1.1 Velocity test

Probably the simplest case to analyze further is the velocity test where v is specified on the (flat) top surface of the sample. Although even the leading order problem is hard to solve, we can analyze the solution for small times. Assuming that $\eta_0(y, 0) = 1$ and $v = -V_T$ on $y = 1$ (where V_T is a non-dimensional velocity), we expand v_0 and η_0 in powers of t and find that the solution which satisfies $v_0 = 0$ on $y = 0$ is given by

$$\eta_0 = 1 + \tfrac{1}{8}t(8V_T - 2\alpha y + \alpha) + O(t^2),$$

$$v_0 = \tfrac{1}{8}\alpha y^2 - y\left(V_T + \tfrac{1}{8}\alpha\right) + \tfrac{1}{192}t\left[\alpha y\left(2\alpha y^2 - 3\alpha y + \alpha - 24V_T y + 24V_T\right)\right] + O(t^2)$$

This solution therefore distinguishes between three values of the speed V_T of the top plate (see figs. 3a, 3b and 3c).

For $V_T > \alpha/8$, the outer problem predicts that both the top and the bottom of the sample will "bulge" as top plate is pushed down. The free boundary is linear, and the horizontal velocity on the top and bottom of the sample is proportional to X. For $V_T = \alpha/8$, the imposed

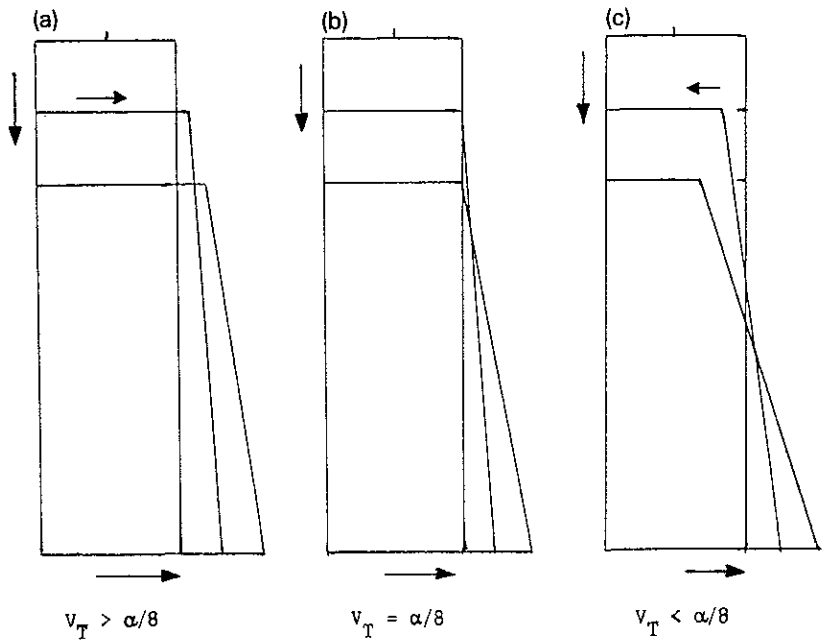

Fig. 3 Development of sample semi-width shapes for various values of V_T (velocity test)

velocity is just enough to preserve the condition that $\eta_0 = 1$ at $y = 1$, so that the horizontal velocity on $y = 1$ is zero. Of course, there is still a non-zero horizontal slip on $y = 0$. In the case $V_T < \alpha/8$, the imposed velocity is not enough to overcome the "slumping" due to gravity. Thus the top of the sample moves towards the y-axis and the bottom away from it. This behaviour is consistent with the early stages of the formation of a liquid drop under gravity, for example.

Near $y = 0$ and $y = s(t)$ the outer solution is not valid and boundary layers must be introduced (see section 3.3). The outer solution may nevertheless be used to estimate the effective viscosity from measurements of the maximum "bulge" in the sample. We find that

$$\eta_0 = 1 + t\left(V_T + \tfrac{1}{8}\alpha\right) + O(t^2)$$

at $y = 0$, and re-dimensionalizing reveals that for a sample of height h, semi-width L and density ρ where the top plate moves with speed U_∞, if the maximum semi-width of the sample at any time is BL, then this is related to the effective viscosity by

$$\mu = h^2 \rho g t / 8\left[h(B-1) - U_\infty t\right].$$

3 1.2. Viscometer

In the case of the viscometer, we must satisfy the boundary conditions $v_0 = 0$ on $y = 0$ and $-p_0 + 2v_{0y} = \gamma(t)$ on $y = s(t)$. The shear stress and the position of the boundary are unknown. For a constant load $\gamma(t) = -\gamma$ say (where γ is non-dimensional), we may again examine the small-time behaviour of the solution, retrieving

$$\eta_0 = 1 + \tfrac{1}{4}t(\gamma - \alpha y + \alpha) + O(t^2),$$

$$v_0 = \tfrac{1}{8}\alpha y^2 - \tfrac{1}{4}y(\gamma + \alpha) + \tfrac{1}{96}t\left[\alpha y(\alpha y^2 - 3\alpha y + 3\alpha - 3\gamma y + 6\gamma)\right] + O(t^2).$$

Here again the "bulge" is linear in y, and for $\gamma > 0$ the picture always resembles that of fig. 3a. The only circumstances under which there is any form of "necking" of the sample occur

when γ is negative so that the top surface of the sample is actually being forced upwards. For this experiment the viscosity can again be estimated by measuring the maximum "bulge" as in the velocity test. The corresponding (dimensional) result is that for a maximum sample semi-width BL and a (dimensional) load Γ,

$$\mu = t(\Gamma + h\rho g)/4(B-1).$$

For the viscometer, the downward speed of the top of the sample is also unknown, and this provides us with an additional means of estimating the viscosity for short times. If we assume that $\eta_0 = 1 + O(t)$, then we may solve eqs. (3) for small times and impose the conditions $v_0 = 0$ on $y = 0$ and $-p_0 + 2v_{0y} = -\gamma$ on $y = s(t)$ to retrieve

$$v_0 = \tfrac{1}{8}\alpha y^2 + y\left[-\tfrac{1}{4}\gamma - \tfrac{1}{4}\alpha s(t)\right].$$

Now using the fact that $v_0 = \dot{s}(t)$ on $y = s(t)$ we find that

$$\dot{s} = -\tfrac{1}{8}\alpha s^2 - \tfrac{1}{4}\gamma s$$

and hence

$$s(t) = 2\gamma\, e^{-\gamma t/4}/(\alpha + 2\gamma - \alpha\, e^{-\gamma t/4}).$$

Re-dimensionalizing, we find that the effective viscosity is given for small times in terms of the position of the top boundary by

$$\mu = \frac{\Gamma t}{4\log[(2h\Gamma + h\rho g s)/s(h\rho g + 2\Gamma)]} \sim \frac{ht(\Gamma + h\rho g/2)}{4(h-s)}.$$

3.1.3. Plasticity test

The plasticity test is complicated by the fact that with no top plate constraining the sample, there is no longer any reason why the top surface should remain flat. Accordingly, we write $u = \tau(x, t)$ to specify the top surface of the sample where τ is non-dimensional. Scaling x and y with ϵ and imposing the stress-free conditions on the top surface reveals that to lowest order we must satisfy

$$\tau_X(p_0 - 2U_{0X}) = 0, \quad -\tau_X(v_{2X} + U_{0y}) - p_0 + 2v_{0y} = 0.$$

Evidently, the first of these conditions is satisfied automatically. The normal stress condition becomes

$$4v_{0y} + X\tau_X(-\alpha + 4v_{0yy}) = 0,$$

and a small time expansion shows that as before

$$\eta_0 = 1 + t\left(-C - \tfrac{1}{4}y\alpha\right) + \tfrac{1}{32}\alpha t^2(8Cy + \alpha y^2 - 4D) + O(t^3),$$

$$v_0 = \tfrac{1}{8}\alpha y^2 + Cy + \tfrac{1}{96}ty(96C^2 + 12C\alpha y + \alpha^2 y^2 + 24\alpha D) + O(t^2),$$

where C and D are constants. Imposing the boundary condition on the top surface $y = 1 + t\tau_1(X) + O(t^2)$ gives that to lowest order $4C + \alpha = 0$, so determining C, and the order t condition determines $\tau_1(X)$ as

$$\tau_1(X) = -D - \tfrac{1}{8}\alpha.$$

Although D may be determined by going to higher orders, we have the information which we need: for small times the top surface remains parallel to the X-axis to leading order. Assuming once again that the maximum "bulge" is that predicted by the outer solution, we find that the effective viscosity for a maximum bulge BL is approximated by

$$\mu = h\rho g t/4(B-1).$$

Using the result that in the plasticity test the top surface remains flat to lowest order, we may also estimate the effective viscosity as in the case of the viscometer by examining the motion of the top boundary. Using the result for the viscometer with $\gamma = 0$, we find that

$$s(t) = 8/(8+\alpha t), \quad \dot{s}(t) = -8\alpha/(8+\alpha t)^2.$$

Re-dimensionalizing reveals that

$$\mu = sh\rho gt/8(h-s).$$

Clearly if we wished to determine the viscosity of the sample via the initial speed of the top surface, then this could also be accomplished, though the formula is somewhat messy.

3.2. *The outer problem for later times*

It is worth making some comments on the solution to the leading order problem for the tall, thin sample at later times. In the case of the velocity test, a search for similarity solutions may be made by seeking stretching transformations to the problem

$$\dot{\eta}_0 + (\eta_0 v_0)_y = 0, \quad (\eta_0 v_{0y})_y = \tfrac{1}{4}\alpha\eta_0,$$

$$v_0 = 0 \quad \text{at} \quad y = 0, \quad v_0 = \dot{s}(t) \quad \text{at} \quad y = s(t).$$

We find that the problem may be rendered invariant if we set $v_0 = \lambda V_0$, $\eta_0 = N_0$, $y = \lambda^{1/2} Y$, $t = \lambda^{-1/2} T$ and $s = \lambda^{1/2} S$, which gives rise to a similarity variable $\zeta = yt$ and a velocity v_0 of the form $v_0 = t^{-2} g(\zeta)$. Of course for consistency $s(t)$ must be a function of t alone, which means that we are forced to take $s(t) = A/t$ where A is a constant. The free surface condition then requires that $g(A) = -A$, giving a boundary condition for g. The form of $s(t)$ represents the limiting case where the sample starts off with infinite height and is compressed by the top plate to zero height in infinite time. If we now assume that $\eta_0 = h(\zeta)$, then the similarity equations and boundary conditions are

$$\zeta h' + (gh)' = 0, \quad (g'h)' = \tfrac{1}{4}\alpha h,$$

$$h(0) = 1, \quad g(0) = 0, \quad g(A) = -A.$$

Although it is possible to eliminate h and retrieve the equation

$$g'' - g'^2/(\zeta + g) = \tfrac{1}{4}\alpha,$$

a numerical solution is required in general. The only case where any progress can be made is when gravity is negligible, so that $\alpha \ll 1$ and $\mu \gg h^2\rho g/U_\infty$. In this case the equations are the same as those considered by Dewynne et al. (1989), who pointed out that they may be solved for arbitrary $s(t)$ by means of a hodograph transformation. We have for $\alpha = 0$

$$\eta_0 v_{0y} = C(t).$$

Defining a scaled time T by

$$T = \int_0^t C(p)\, \mathrm{d}p$$

and writing $v_0 = C(t)V_0$, the equations become

$$\eta_{0T} + V_0\eta_{0y} = -1, \quad \eta_0 V_{0y} = 1 \quad (\eta_0(y,0) = \eta_{0i}(y), V_0(0,T) = 0).$$

Eliminating the variable V_0 and employing a hodograph transformation to change from $\eta_0 = \eta_0(y, T)$ to $y = y(\eta_0, T)$ gives the equation

$$y_{\eta_0} = \eta_0(y_{\eta_0 T} - y_{\eta_0\eta_0}),$$

which is a first-order quasi-linear equation for y_{η_0}. Assuming that the initial condition $\eta_0 = \eta_{0i}(y)$ at $T = t = 0$ may be solved to give say $y = y_{0i}(\eta_0)$ at $T = 0$, and setting $(y_{0i})_{\eta_0} = z_{0i}(\eta_0)$, we find that η_0 is given implicitly by

$$\eta_{0y} = \eta_0/(\eta_0 + T)\, z_{0i}(\eta_0 + T).$$

In principle therefore the problem is solved for arbitrary $s(t)$ and $\eta_{0i}(y)$ since the relationships

$$\mathrm{d}T/\mathrm{d}t = \dot{s}(t)/V_0(s(t), t), \quad \eta_0(0, T) + T = \eta_{0i}(0)$$

completely determine the solution. In practice of course all the relationships are implicit so the solution is somewhat awkward to handle. The simplest case is that of an initially straight-sided sample so that $\eta_{0i} = 1$, whence

$$\eta_0(t) = s(0)/s(t), \quad v_0 = [\dot{s}(t)/s(t)]\, y,$$

so that the sample always assumes a rectangular shape and is slowly squashed to zero height. This solution is of little practical use however as it gives no information about the viscosity – evidently the force required to push the top plate down with a given velocity would vary according to the viscosity. If however we prescribe the normal stress $-\gamma(t)$ on the top plate, then the relevant solution is

$$\eta_0(t) = \exp\left(\int_0^t \tfrac{1}{4}\gamma(\xi)\, \mathrm{d}\xi\right), \quad v_0 = -\tfrac{1}{4}\gamma(t)y, \quad s(t) = \exp\left(-\int_0^t \tfrac{1}{4}\gamma(\xi)\mathrm{d}\xi\right)$$

and again the viscosity may be estimated by either the bulge in the sample or the speed of the top plate.

3.3. *The boundary layer near the base of the sample*

It was noted above that near the base or top of the sample the outer problem is not valid and a rescaling is required to allow the full boundary conditions to be satisfied. Although the outer solution derived in section 3.1. will be sufficient to estimate the viscosity, completeness demands that the boundary layer structure should be analyzed to confirm that the matching problem can at least be solved in principle.

Considering first the base of the sample, it is easily shown that if in addition to the scalings already chosen for U and X we introduce new variables Y and V where $y = \epsilon^n Y$, $v = \epsilon^n V$, then only a choice of $n = 1$ will not either lead back to the outer problem, or lead to a problem where the full no-slip condition cannot be satisfied. The choice of $n = 1$ leaves eqs (1) as

$$p_X = U_{XX} + U_{YY}, \quad p_Y = V_{XX} + V_{YY} - \epsilon\alpha, \quad U_X + V_Y = 0, \tag{4}$$

with boundary conditions $U = V = 0$ on $Y = 0$, symmetry on $X = 0$, stress-free on $X = \eta(Y, t)$ and satisfying matching conditions with the outer solution as $Y \to \infty$. For brevity we only consider the region near to the base of the sample, but the boundary layer near to the top of the sample may be investigated via similar techniques. Evidently (4) is the full Stokes flow problem and moreover for arbitrary times the free boundary is in motion, so that in general an analytic solution will not be possible and we will have to resort to numerical methods. Again, however the problem may be solved for small times.

3.3.1 *The matching problem for small times*

Concentrating for the present moment on the details of the velocity test (the other two cases may be analyzed similarly), we may exploit the fact that for small times the free

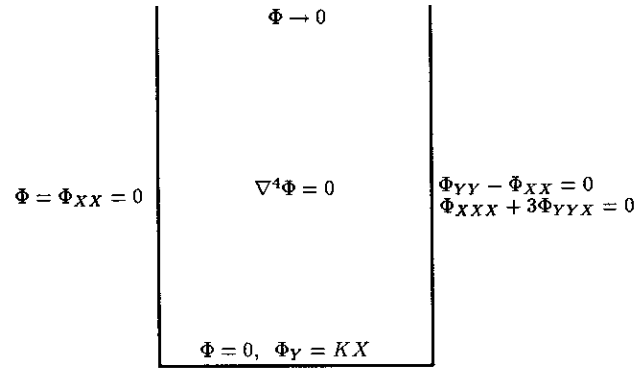

Fig. 4. Matching problem near base of sample

boundary S_+ of the sample remains vertical, and the outer velocity is known in the form

$$v_0 = -X\left[\tfrac{1}{8}\alpha y^2 + Ky\right] + O(t),$$

where K denotes the constant $-V_T - \alpha/8$. Introducing a stream function Ψ which has also been scaled with ϵ, the matching problem for small times becomes

$$\nabla^4\Psi = 0, \quad 0 \le X \le 1, \quad 0 \le Y < \infty,$$

with boundary conditions

$$\Psi = \Psi_{XX} = 0 \quad \text{on} \quad X = 0,$$

$$\Psi = \Psi_Y = 0 \quad \text{on} \quad Y = 0,$$

$$\Psi_{YY} - \Psi_{XX} = \Psi_{XXX} + 3\Psi_{XYY} + \epsilon\alpha = 0 \quad \text{on} \quad X = 1$$

and matching condition

$$\Psi = -X\left(\tfrac{1}{8}\alpha\epsilon Y^2 + KY\right) \quad \text{as} \quad Y \to \infty.$$

Subtracting out the behaviour at $Y = \infty$ by setting $\Psi = -KYX + \Phi$ and considering the problem only to lowest order in ϵ, we finally require to solve the problem shown in fig. 4.

This problem for the biharmonic equation may be solved by separation of variables. Assuming solutions of the form

$$\Phi = \Theta_1(X)\Theta_2(Y),$$

it may easily be shown that the conditions at $Y = \infty$ require Θ_1 and Θ_2 to be chosen in the form

$$\Theta_1(X) = AX \sin \lambda X + BX \cos \lambda X + C \sin \lambda X + D \cos \lambda X,$$

$$\Theta_2(Y) = \exp(-\lambda Y)$$

and we must now impose the boundary conditions. The symmetry conditions force $A = D = 0$, whilst for non-zero eigenvalues λ the conditions on the free surface lead to

$$B[\cos \lambda + (\sin \lambda)/\lambda] + C \sin \lambda = 0, \quad B \sin \lambda - C \cos \lambda = 0$$

Equating the determinant of the coefficient matrix to zero in the usual way gives the eigenvalue equation

$$\lambda + \sin \lambda \cos \lambda = 0,$$

which identifies the λ_n as the Papkovitch–Fadle eigenvalues, first identified by Papkovitch (1940) and Fadle (1940). It is clear that a given eigenvalue λ_n immediately gives rise to three

Table 1
First five Papkovitch–Fadle eigenvalues.

n	$\mathrm{Re}(\lambda_n)$	$\mathrm{Im}(\lambda_n)$
1	2.10620	1.12536
2	5.35627	1.55157
3	8.53668	1.77554
4	11.69918	1.92940
5	14.85406	2.04685

others, namely $-\lambda_n$, $\bar{\lambda}_n$ and $-\bar{\lambda}_n$, so that there is one family of (non-zero) eigenvalues in each quadrant of the complex plane. We are interested only in those eigenvalues with $\mathrm{Re}(\lambda_n) > 0$, and this doubly infinite family may easily be determined by simple Newton–Raphson iteration. For example, the first five such eigenvalues are given (to 5 d.p.) in table 1.

The asymptotic distribution of the eigenvalues is easily determined (see, for example Spence (1982)) and is given by

$$\lambda_k = \left(k - \tfrac{1}{2}\right)\pi + \tfrac{1}{2}\mathrm{i}\,\log(4k\pi) + \mathrm{O}(\log\, k/k)$$

If we now write the eigenfunction expansion for Φ as

$$\Phi(X, Y) = \sum_n c_n \phi_n(X)\, \mathrm{e}^{-\lambda_n Y}$$

where the eigenfunctions have been defined by

$$\phi_n(X) = \left(\lambda_n \cos^2 \lambda_n\right)^{-1}(X \cos \lambda_n \cos \lambda_n X + \sin \lambda_n \sin \lambda_n X)$$

(the scaling factor has been included for convenience), then it only remains to determine the coefficients c_n so that

$$0 = \sum_n c_n \phi_n(X), \quad KX = \sum_n -\lambda_n c_n \phi_n(X).$$

The fact that the eigenvalues are complex allows us the freedom to satisfy these conditions for the c_n, since the c_n themselves will be complex. The task is not quite as simple as it may at first appear however, because the eigenfunctions $\phi_n(X)$ are not mutually orthogonal. It turns out that problems of this sort for the biharmonic equation fall naturally into two classes, which have come to be known as *canonical* and *non-canonical* end problems. Some explanation of these two classes of problems is apposite.

For a moment, let us consider some slightly more general problems than the one which was posed above. Classically, end problems for the biharmonic strip have normally appeared in two guises: problems for slow viscous flow in a semi-infinite trench (see, for example Liu and Joseph (1977)) where the biharmonic function Ψ represents a stream function; and problems in elasticity where the region in question is considered to be a semi-infinite linear elastic strip (see, for example Smith (1952) or Horvay (1957)) and the biharmonic function is an Airy stress function. In both these form of the problem, the conditions are normally taken to be no slip (Stokes flow) or no displacement (elasticity) on the long sides of the strip, rather than the stress-free conditions which pertain in our problem. The conditions on $y = 0$ are typically composed of prescribing some combination of stresses and accelerations (Stokes flow) and some combination of stresses and displacements (elasticity), rather than the velocity conditions which we wish to impose. Using the convenient notation of Spence (1978), we define the functions $f_1(X)$, $f_2(X)$, $f_3(X)$ and $f_4(X)$ by

$$f = \left(f_1(X), f_2(X), f_3(X), f_4(X)\right) = \left(\Phi_{XY}, \Phi_{XX}, Q, P\right)|_{Y=0},$$

where $P = \nabla^2 \Phi$ and Q is the harmonic conjugate of P. Then we may express boundary conditions at $Y = 0$ for all the problems discussed above in terms of combinations of elements of f. Using the eigenfunction expansion, we may also define functions ϕ_{nk} $(k = 1, 4)$ by

$$f_k(X) = \sum_n c_n \phi_{nk}(X),$$

so that

$$\begin{pmatrix} \phi_{n1}(X) \\ \phi_{n2}(X) \\ \phi_{n3}(X) \\ \phi_{n4}(X) \end{pmatrix} = \begin{pmatrix} \left(\lambda_n \sin \lambda_n X - \cos^2 \lambda_n \cos \lambda_n X\right)/\cos \lambda_n \\ \left[-\lambda_n \cos \lambda_n X + \left(\sin^2 \lambda_n - 2\right) \sin \lambda_n X\right]/\cos \lambda_n \\ -2 \sin \lambda_n X/\cos \lambda_n \\ 2 \cos \lambda_n X/\cos \lambda_n \end{pmatrix}.$$

Consider now for definiteness the problem where the prescribed functions on $Y = 0$ are $f_1(X)$ and $f_3(X)$. Then although in general we cannot find functions which are orthogonal to ϕ_{n1}, if we can find functions $\beta_{m1}(X)$ and $\beta_{m3}(X)$ such that

$$\langle \beta_{m(1,3)}, \phi_{n(1,3)} \rangle = \delta_{mn},$$

where we have defined the inner product by

$$\langle a_{(p,q)}, b_{(p,q)} \rangle = \int_0^1 \left(a_p b_p + a_q b_q\right) \mathrm{d}X,$$

the coefficients c_n will be determined completely via the quadrature

$$c_m = \langle f_{(1,3)}, \beta_{m(1,3)} \rangle.$$

For the case of f_1 and f_3 prescribed, this may be accomplished, as it turns out that β_{m1} is a multiple of ϕ_{m3} and β_{m3} is a multiple of ϕ_{m1}. Such functions β_m are usually termed *biorthogonal* functions. The crucial point however is that such biorthogonal functions do not always exist. In fact it is easy to show that suitable biorthogonal functions *only* exist in the cases when f_1 and f_3 are prescribed, and when f_2 and f_4 are prescribed. Problems with this data are therefore termed *canonical*, and their solutions may be written down in terms of quadratures. There are also results available on completeness and convergence (see, for example Gregory (1980)). Problems with any other data prescribed are termed *non-canonical*, and are therefore much harder to solve.

Returning to the specific problem which we wish to solve, the data prescribed is Φ and Φ_Y. This amounts to f_1 and f_2 in the notation introduced above, so that the problem is a non-canonical one. Although the coefficients c_n may not be determined explicitly, it is possible to solve the problem using collocation. The easiest way to do this is to write

$$\beta_{m1} = A\phi_{m1} + B\phi_{m2}, \quad \beta_{m2} = C\phi_{m3} + D\phi_{m4},$$

where A, B, C and D are constants. Forming an inner product with the prescribed data then gives

$$c_m = \sum_n H_{mn} c_n + d_n,$$

where

$$d_m = \langle \beta_{m(1,2)}, f_{(1,2)} \rangle,$$

$$H_{mn} = \delta_{mn} - \int_0^1 \left(\beta_{m1}\phi_{n1} + \beta_{m2}\phi_{n2}\right) \mathrm{d}X.$$

This gives rise to an infinite set of linear equations for the c_m which are to be solved by

truncation. The introduction of the constants A, B, C and D was first used by Spence (1978) and represents an improvement on all previous collocation methods for this problem as the choice $A = -1$, $C = 1$, $B = 1/2$ and $D = -1/2$ (giving rise to "optimal weighting functions") renders the system of equations diagonally dominant, which is the crucial property ensuring that as $n \to \infty$ the solution to the truncated $n \times n$ system of equations tends to the exact solution of the equations (see, for example Kantorovitch and Krylov (1958)). It is also possible to derive asymptotic estimates for the coefficients.

We therefore conclude that the matching problem at the bottom of the sample (and, with some insignificant changes in boundary conditions the top of the sample) is well-defined, at least for small times, and in principle may be solved via collocation. The initial movement of the free boundary of the sample may also be calculated, giving

$$\eta_0 = 1 + t\eta_1(Y) + O(t^2),$$

where

$$\eta_1(Y) = \sum_n c_n \sec^2\lambda_n[1 - \exp(-\lambda_n Y)],$$

so that, as expected, the boundary exhibits a "bulge" as we move away from $Y = 0$, subject of course to the usual condition on α

It is worth remarking that the eigenfunction expansion could be used to determine the (unknown) coefficients for the corner solution eigenfunctions discussed in section 2.1. In practice though this would lead to an infinite system of linear equations where the matrix is full and not diagonally dominated. The conclusion here is that although the corner solutions give interesting qualitative results concerning the nature of the "bulging", they do not provide useful quantitative results; for these we might as well solve the full boundary layer problem as indicated above

4. Numerical methods for the full problem

In the previous section we have seen that the full problem involves solving the time-independent slow flow equations, and then advancing the position of the free surface using a kinematic condition.

We will solve the problem numerically using a combination of Lagrangian and Eulerian methodologies. The solution will be calculated at a series of discrete points in time. At the beginning of each time step it is assumed that the current position of the free surface, and hence the shape of the flow region, is known. An Eulerian formulation of the slow flow equations will be solved using the finite element method. This will yield values for the velocity components at a set of points inside and on the boundary of the flow region. These points will then be moved as in a Lagrangian formulation to give the position of the flow region at the next time level.

A similar combined Eulerian–Lagrangian technique which used a boundary element method to calculate the solution to the slow flow equations on the boundary of the flow region would also be suitable. For the particular case of Stokes flow with constant viscosity the boundary element method is probably more efficient than a finite element method, but it does not yield information about the flow in the interior of the region nor would it cope so easily with an extended model in which the viscosity is not constant.

4.1. Finite element solution of the slow flow equations

The slow flow equations described earlier may be solved for arbitrary initial shapes using the finite element method. This is most conveniently used when the equations of motion are

written in terms of the primitive variables p, u and v, where the velocity $\boldsymbol{q}$ has been written $\boldsymbol{q} = u\boldsymbol{i} + v\boldsymbol{j}$. To allow the free surface stress conditions to be applied, the equations are best taken in the form

$$\partial t_{xx}/\partial x + \partial t_{xy}/\partial y = 0, \quad \partial t_{yx}/\partial x + \partial t_{yy}/\partial y = \alpha, \tag{5}$$

$$\partial u/\partial x + \partial v/\partial y = 0, \tag{6}$$

where the stress components are defined by

$$t_{xx} = -p + 2\,\partial u/\partial x, \quad t_{xy} = t_{yx} = \partial u/\partial y + \partial v/\partial x,$$

$$t_{yy} = -p + 2\,\partial v/\partial y.$$

The x and y components of the surface traction across a free surface with outward normal n are

$$T_x = t_{xx}\,\partial x/\partial n + t_{xy}\,\partial y/\partial n, \quad T_y = t_{yx}\,\partial x/\partial n + t_{yy}\,\partial y/\partial n.$$

All the paste samples considered in this study are symmetrical about the line $x = 0$ Therefore for computational purposes we will consider only the right hand half of the flow region and introduce a new boundary S_A (the axis of symmetry) on $x = 0$. The boundary conditions in this formulation are written as

$$u = v = 0 \quad ((x, y) \in S_B), \quad T_x = T_y = 0 \quad ((x, y) \in S_+),$$

$$u = T_y = 0 \quad ((x, y) \in S_A)$$

and, for $(x, y) \in S_T$,

$$T_x = T_y = 0 \quad \text{(plasticity test)},$$

$$u = 0, \quad v = \dot{s}(t) \quad \text{(velocity test)},$$

$$u = 0, \quad T_y = \gamma(t) \quad \text{(viscometer test)}.$$

The flow region D is divided into triangular elements with corner and midside nodes. Following normal practice the velocity components will be approximated by a polynomial on each element which is one degree higher than that used for the pressure. Here a linear approximation for the pressure is used (using the corner nodes only) and quadratic approximations are used for u and v (using all the nodes). Specifically, we let

$$u \approx \tilde{u} = \sum_{i=1}^{N} u_i \phi_i(x, y), \quad v \approx \tilde{v} = \sum_{i=1}^{N} v_i \phi_i(x, y), \quad p \approx \tilde{p} = \sum_{i=1}^{M} p_i \psi_i(x, y),$$

where $\phi_i(x, y)$, $i = 1, \ldots, N$ and $\psi_i(x, y)$, $i = 1, \ldots, M$ are given quadratic and linear basis functions respectively, and u_i, v_i, $i = 1, \ldots, N$ and p_i, $i = 1, \ldots, M$ are nodal values for u, v and p.

The functions $\tilde{u}$, $\tilde{v}$ and $\tilde{p}$ are chosen to satisfy the the weak form of eqs. (5), (6) as follows:

$$\iint_D \left(-\frac{\partial}{\partial x}(\tilde{t}_{xx}) - \frac{\partial}{\partial y}(\tilde{t}_{xy}) \right) \phi_i \, dx \, dy = 0, \quad i = 1, \ldots, N, \tag{7}$$

$$\iint_D \left(\alpha - \frac{\partial}{\partial x}(\tilde{t}_{yx}) - \frac{\partial}{\partial y}(\tilde{t}_{yy}) \right) \phi_i \, dx \, dy = 0, \quad i = 1, \ldots, N, \tag{8}$$

$$\iint_D \left(\frac{\partial \tilde{u}}{\partial x} + \frac{\partial \tilde{v}}{\partial y} \right) \psi_i \, dx \, dy = 0, \quad i = 1, \ldots, M. \tag{9}$$

Note that if a particular u_i or v_i is given as a boundary condition, then the corresponding equation is deleted from the set (7) or (8) above.

Applying the divergence theorem to (7) and (8) above gives

$$\int\int_{\mathrm{D}}\left(\tilde{t}_{xx}\frac{\partial\phi_i}{\partial x}+\tilde{t}_{xy}\frac{\partial\phi_i}{\partial y}\right)\mathrm{d}x\,\mathrm{d}y-\int_{\mathrm{S}}T_x\phi_i\,\mathrm{d}S=0,\quad i=1,\ldots,N, \tag{10}$$

$$\int\int_{\mathrm{D}}\left(\alpha\phi_i+\tilde{t}_{yx}\frac{\partial\phi_i}{\partial x}+\tilde{t}_{yy}\frac{\partial\phi_i}{\partial y}\right)\mathrm{d}x\,\mathrm{d}y-\int_{\mathrm{S}}T_y\phi_i\,\mathrm{d}S=0,\quad i=1,\ldots,N, \tag{11}$$

respectively, where S is the complete boundary of the region D.

The surface integral makes the imposition of the boundary conditions very straightforward. Consider the boundary conditions for eq. (10) at a particular node i, on the boundary S. Either u_i is given as a boundary condition (on $\mathrm{S_B}$, $\mathrm{S_A}$ and possibly $\mathrm{S_T}$), in which case the equation is deleted from the set, or $T_x=0$ and so the surface integral is zero. A similar argument applies to eq. (11), except for the case of the viscometer test, when the surface integral has a non-zero but *prescribed* value for points on $\mathrm{S_T}$.

Substituting for

$$\tilde{t}_{xx}=-\sum_{i=1}^{M}p_i\psi_i+2\sum_{i=1}^{N}u_i\,\partial\phi_i/\partial x,$$

$$\tilde{t}_{yx}=\tilde{t}_{xy}=\sum_{i=1}^{N}\left(u_i\,\partial\phi_i/\partial y+v_i\,\partial\phi_i/\partial x\right),$$

$$\tilde{t}_{yy}=-\sum_{i=1}^{M}p_i\psi_i+2\sum_{i=1}^{N}v_i\,\partial\phi_i/\partial y$$

into eqs. (9), (10) and (11) gives $(2N+M)$ linear algebraic equations for the nodal values u_i, v_i, $i=1,\ldots,N$ and p_i, $i=1,\ldots,M$.

4.2. Advancing through time

In the previous section the time variable was not explicitly used, but by applying the ideas of that section at a particular time t we solve the following problem:

Given $\mathrm{D}(t)$, the flow region at time t, calculate u, v and p as functions of x and y, but also implicitly as functions of t. We now use the Lagrangian equations

$$\mathrm{d}x/\mathrm{d}t=u,\quad \mathrm{d}y/\mathrm{d}t=v,$$

to advance the position of points in $\mathrm{D}(t)$. Specifically we take each corner node of the triangularisation of the previous section and advance using explicit time differencing as follows

$$x_i(t+\delta t)=x_i(t)+u_i\delta t,\quad y_i(t+\delta t)=y_i(t)+v_i\delta t.$$

These new nodal positions define the region $\mathrm{D}(t+\delta t)$, and the whole process may be repeated.

Evidently it is not essential to apply the Lagrangian equations of motion to all the internal nodes of D. The free surface could be tracked using the boundary nodes only, and then the new area could be re-triangulated. However much of the work involved in applying the finite element method to slow flow equations at each time step involves "house-keeping" operations such as the building or maintenance of lists of element/node connections. Using the technique described here, where all the corner nodes are moved at each time step, maintains

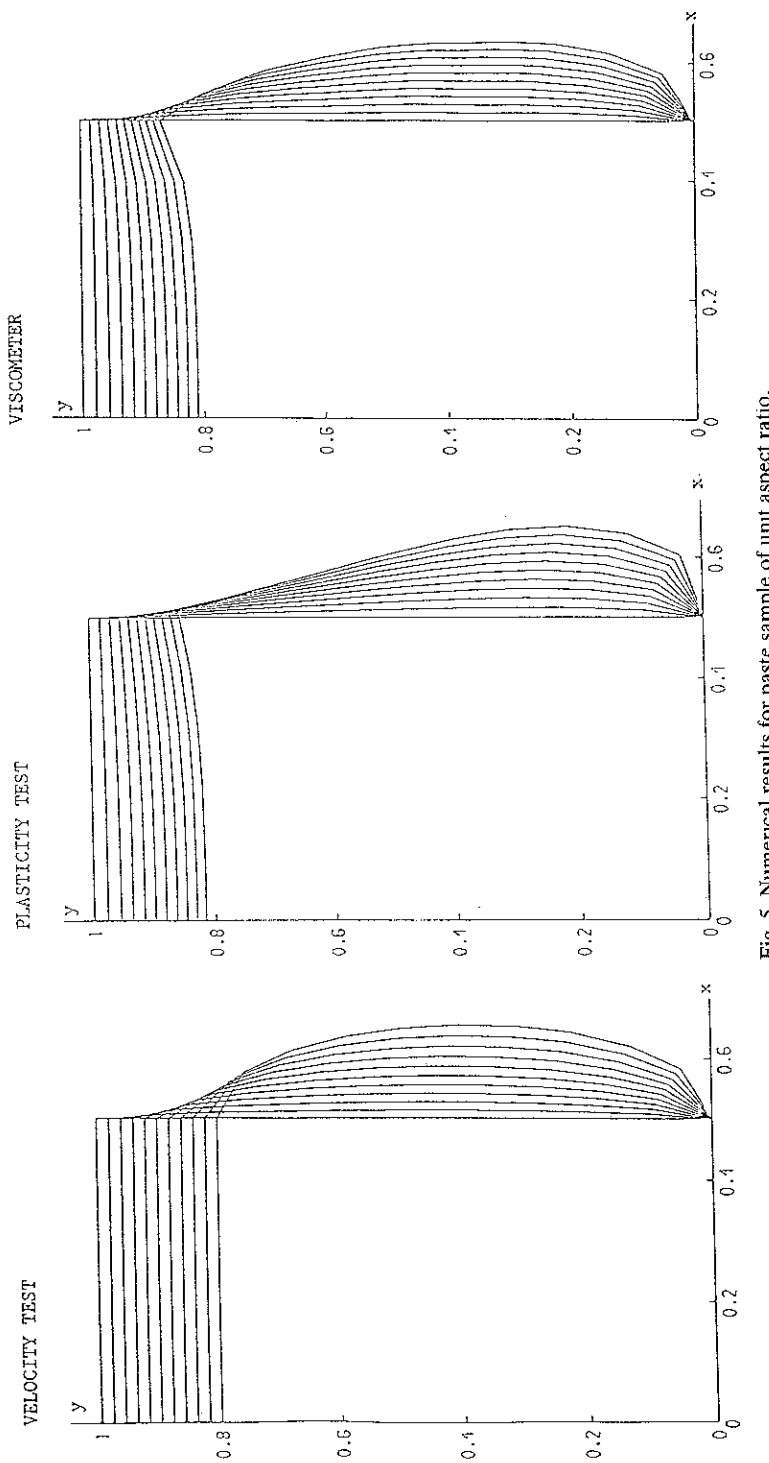

Fig. 5. Numerical results for paste sample of unit aspect ratio.

the topology of the element layout from one step to the next and so reduces the finite element overheads.

The mid-side nodes are not updated directly, since this could lead to the creation of triangles with curved sides, but this does not increase the overheads since the topology is determined by corner nodes.

5. Numerical results

The numerical method described above was used to give predictions of the shape of a paste sample undergoing the velocity, plasticity or viscometer tests. The cases considered included both samples where the aspect ratio was chosen so that the analysis of section 3 applied, and order one aspect ratios where the theory is not valid.

In all of the calculations reported below the paste sample had a viscosity of $\mu_p = 10^8$ Pa s and a density of 3000 kg/m^3. The gravitational constant g was taken as 9.8 m/s^2, and the velocity scale was 1 m/h.

The accuracy of the numerical solution of the mathematical model is controlled by the size of the elements and the size of the time step. There is a further constraint on the size of the time step for any given element size to maintain numerical stability for the explicit time-stepping. Calculations were performed for a variety of space and time steps and different calculated values of the key output variables, namely the maximum bulge and the sample height, were compared. Using a simple test of consistency it was found that the use of 100 elements (giving 231 nodes and 528 variables) gave an error of order 10^{-4} in these variables. The appropriate value of the time step depends on the problem being solved, since the imposition of different boundary conditions gives a different time scale to the problem. Using the same consistency test it was found that time increments of 0.02, 0.2 and 0.07 h were suitable for the velocity, plasticity and viscometer tests respectively. The results presented below use these values.

It is clear from the graphical results that a smaller element size would have improved the representation of the free surface. However it was not felt appropriate to solve the mathematical equations to a high degree of accuracy, when they represent a simplified model of the real physical situation.

In each of figures 5, 6 and 7 the paste sample had an initial height of 1 m. Figure 5 shows results of the velocity ($V_T = 1$), plasticity and viscometer test ($\gamma = 1$) respectively for the case where the half-width of the base of the sample was 0.5 m. The theory of section 3 predicts the following values of the viscosity of the paste sample shown in table 2. (In table 2, n denotes the number of time increments which have taken place, whilst VE, PB, Ps, VIB and VIs each

Table 2
Numerical results corresponding to fig. 5

n	VE	PB	Ps	VIB	VIs
1	0.4357	1.6569	1.1697	1.2992	1.1985
2	0.4019	1.6653	1.1703	1.3006	1.2023
3	0.3726	1.6740	1.1708	1.3023	1.2059
4	0.3471	1.6831	1.1711	1.3044	1.2095
5	0.3248	1.6927	1.1714	1.3069	1.2131
6	0.3051	1.7029	1.1717	1.3098	1.2168
7	0.2878	1.7136	1.1721	1.3131	1.2208
8	0.2725	1.7251	1.1727	1.3171	1.2251
9	0.2589	1.7375	1.1735	1.3216	1.2297
10	0.2468	1.7509	1.1747	1.3268	1.2348

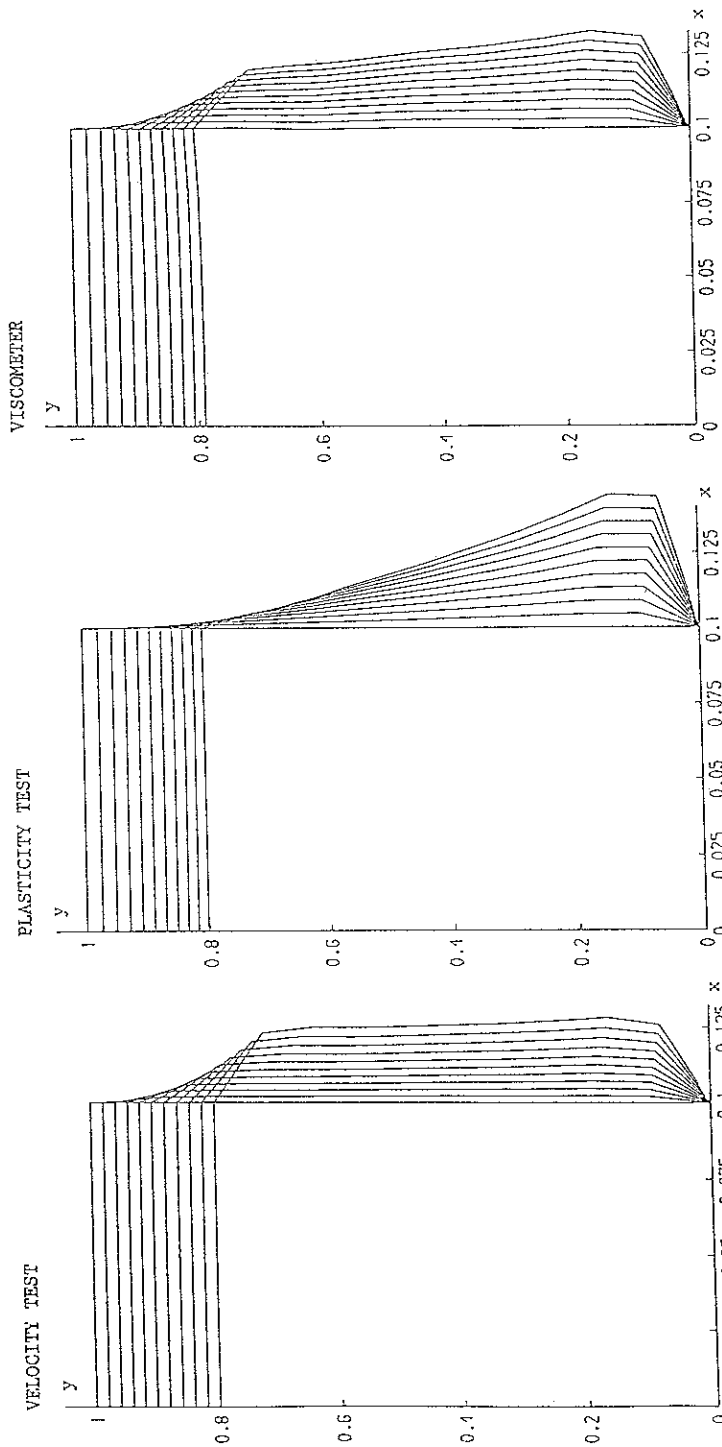

Fig. 6. Numerical results for paste sample of aspect ratio 1/5.

Table 3
Numerical results corresponding to fig. 6.

n	VE	PB	Ps	VIB	VIs
1	0.8304	1.1852	1.0283	1.0914	1.0277
2	0.7258	1.1867	1.0352	1.0902	1.0363
3	0.6416	1.1886	1.0417	1.0889	1.0048
4	0.5724	1.1908	1.0479	1.0876	1.0531
5	0.5145	1.1934	1.0537	1.0861	1.0611
6	0.4653	1.1964	1.0591	1.0846	1.0689
7	0.4232	1.1999	1.0642	1.0831	1.0765
8	0.3867	1.2024	1.0689	1.0815	1.0839
9	0.3547	1.1998	1.0733	1.0800	1.0910
10	0.3266	1.1973	1.0773	1.0785	1.0979

denote the ratio μ/μ_P where μ is the theoretically predicted viscosity from respectively the velocity test, the plasticity test where the maximum bulge is measured, the plasticity test where the sample height is measured, the viscometer test where the maximum bulge is measured and the viscometer test where the sample height is measured.)

Since ϵ is effectively unity in this case, the theory of section 3 is not valid and we expect the results to be poor. Nevertheless, the theoretical values of the viscosity are certainly the correct order of magnitude.

In fig. 6 the geometry of the paste sample is altered so that the base half-width is 0.1 m. A greater degree of bulging is apparent near to the base of the sample. The theoretical

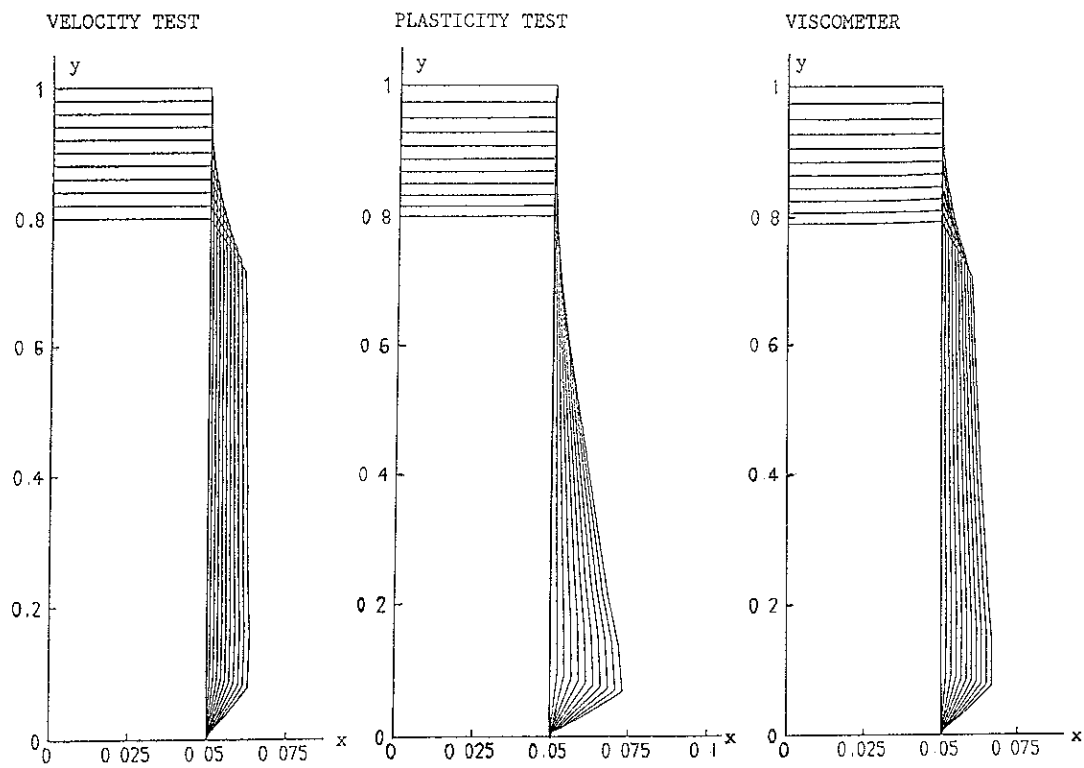

Fig. 7 Numerical results for paste sample of small aspect ratio.

Table 4
Numerical results corresponding to fig. 7

n	VE	PB	Ps	VIB	VIs
1	0.9558	1.1693	1.0089	1.0901	1.0139
2	0.8287	1.1659	1.0160	1.0905	1.0231
3	0.7279	1.1624	1.0228	1.0908	1.0320
4	0.6460	1.1591	1.0293	1.0911	1.0409
5	0.5782	1.1559	1.0357	1.0913	1.0496
6	0.5211	1.1529	1.0418	1.0913	1.0581
7	0.4723	1.1501	1.0476	1.0912	1.0666
8	0.4301	1.1476	1.0533	1.0911	1.0749
9	0.3933	1.1453	1.0587	1.0907	1.0831
10	0.3609	1.1434	1.0640	1.0896	1.0911

predictions of the viscosity shown in table 3 indicate that for the plasticity and viscometer tests acceptable accuracy is produced; when the height of the sample is measured in the plasticity test, the error is less than 5% during the first four time intervals.

In fig. 7 (see also table 4) the half-width of the sample has been reduced to 0.05 m, but all other parameters are the same as in fig. 6. As expected, there is an improvement in the results. Bearing in mind the fact that the effective viscosity of paste samples may change over orders of magnitude as the temperature changes, it is clear from the results below that the theory is easily sufficiently accurate to provide a powerful means of producing useful temperature/viscosity relationships. The results also suggest other useful general guidelines

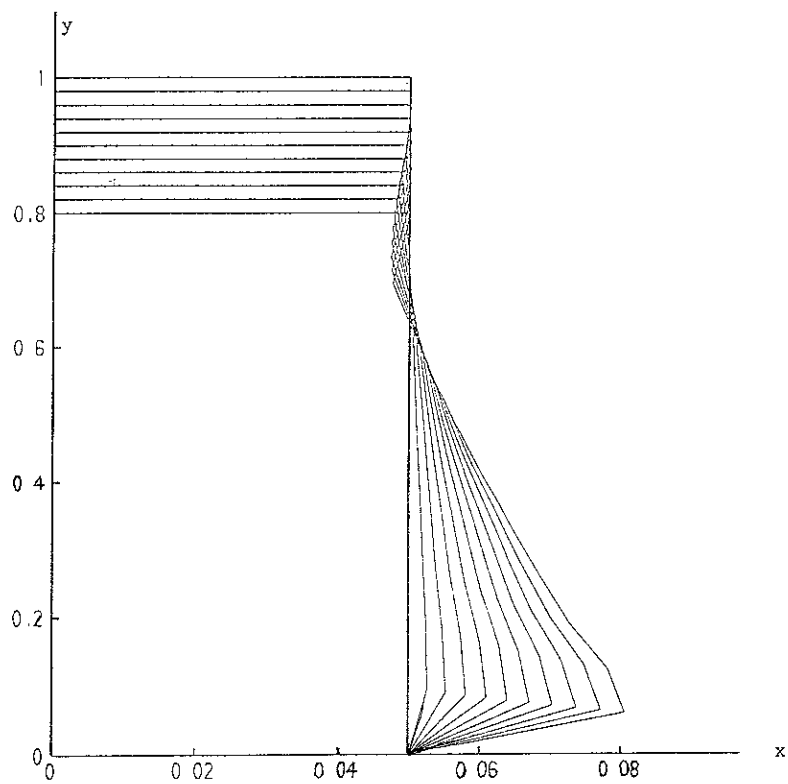

Fig. 8. Numerical results for velocity test showing "necking" of sample

for the experimentalist; the plasticity and viscometer tests are to be preferred over the velocity test, and the height of the sample should be used rather than the maximum bulge.

Finally, fig. 8 shows the particular case where the velocity test was used, but the velocity of the top of the sample was chosen so that $V_T < \alpha/8$. The initial height of the block was 4 m, the base half-width was 0.2 m, and the velocity of the top of the sample was 1 m/h. This gave a value of α equal to 16.9344. The behaviour predicted by the theory of section 3 is clearly illustrated; the sample "necks" whilst spreading out rapidly near to its base.

6. Conclusions

The problem of determining the apparent viscosity of a block of carbon paste used in an important industrial process has been attacked using both analytical and numerical methods. The structure of the flow has been determined using matched asymptotic expansions, and some simple exact solutions have been given for a variety of cases. In these cases, a comparison between the theory and a direct numerical solution exhibited good agreement. In general however the problem must be solved numerically, and the method which has been developed is able to accomplish this efficiently and accurately. Only the two-dimensional case has been considered, but by making some fairly trivial changes to the analysis and numerics, the axisymmetric case could also be considered.

Acknowledgement

Thanks are due to Dr. Svenn A. Halvorsen (Elkem a/s, Kristiansand, Norway), who first brought the problem to our attention at the 1988 Study Group with Industry, Heriot-Watt University. We are also grateful to Dr. P. Wilmott of Oxford University for many helpful discussion and to the referees for their useful suggestions and comments.

References

Bergstrom, T., S. Cowley, A.C. Fowler and P.E. Seward (1989) Segregation of carbon paste in a smelting electrode, *IMA J. Appl. Math. 43*, 83–99.

Dewynne, J., J.R. Ockendon and P. Wilmott (1989) On a mathematical model for fibre tapering, *SIAM J. Appl. Math. 49*, 983–990.

Fadle, J. (1940) Die Selbstspannungs-Eigenwertfunktionen der quadrastischen Scheibe, *Ingr. Arch. 11*, 125–148.

Gregory, R.D. (1980) The traction boundary value problem for the elastostatic semi-infinite strip; existence of solution, and completeness of the Papkovitch–Fadle eigenfunctions, *J. Elasticity 10*, 295–327.

Horvay, G. (1957) Some mixed boundary value problems for the semi-infinite strip, *J. Appl. Mech. 24*, 261–268.

Kantorovitch, L.V. and V.I. Krylov (1958) *Approximate Methods of Higher Analysis* (Noordhof, Groningen).

Liu, C.H. and D.D. Joseph (1977) Stokes flow in wedge-shaped trenches, *J. Fluid. Mech. 80*, 443–463.

Papkovitch, P.F. (1940) Uber eine Form der Losung des Biharmonischen Problems fur das Rechteck, *C. R. (Dokl.) Acad. Sci. URSS 27*, 335–338.

Penney, W.G. and C.K. Thornhill (1952) The dispersion, under gravity, of a column of fluid supported on a rigid, horizontal plane, *Phil. Trans. R. Soc. A 244*, 285–311.

Smith, R.C.T. (1952) The bending of a semi-infinite strip, *Austr. J. Sci. Res. Ser. A 5*, 227–237.

Spence, D.A. (1978) Mixed boundary value problems for the elastic strip: the eigenfunction expansion, *Technical Summary Report 1863*, Mathematics Research Centre, University of Wisconsin, Madison.

Spence, D.A. (1982) A note on the eigenfunction expansion for the elastic strip, *SIAM J. Appl. Math. 42*, 155–173.